Dynamic Error Suppression of Inertial Measurement Unit Based on Improved Unscented Kalman Filter

LI Na[1], *LI Kun*[1], *HE Haiyu*[2*], *JING Min*[3]

1. School of Mathematics and Computer Science, Shaanxi University of Technology, Hanzhong 723000, P. R. China;
2. Trine Engineering Institute, Shaanxi University of Technology, Hanzhong 723000, P. R. China; 3. School of Mechanical Engineering, Shaanxi University of Technology, Hanzhong 723000, P. R. China

(Received 24 March 2025; revised 13 October 2025; accepted 20 November 2025)

Abstract: In this paper, an algorithm on measurement noise with adaptive strong tracking unscented Kalman filter (ASTUKF) is advanced to improve the precision of pose estimation and the stability for data computation. To suppress high-frequency noise, an infinite impulse response filter (IIRF) is introduced at the front end of ASTUKF to preprocess the original data. Then the covariance matrix of the error is corrected and the measurement noise is estimated in the process of filtering. After that, the data from the experiment were tested on the hardware experiment platform. The experimental results show that compared to the traditional extended Kalman filter (EKF) and unscented Kalman filter (UKF) algorithms, the root mean square error (RMSE) of the roll axis results from the algorithm proposed in this paper is respectively reduced by approximately 57.5% and 36.1%; the RMSE of the pitch axis results decreases by nearly 58.4% and 51.5%, respectively; and the RMSE of the yaw axis results decreases almost 62.8% and 50.9%, correspondingly. The above results indicate that the algorithm enhances the ability of resisting high-frequency vibration interference and improves the accuracy of attitude solution.

Key words: accelerometer; inertial measurement unit; adaptive strong tracking unscented Kalman filter (ASTUKF); quaternion; Kalman filter

CLC number: TP212 **Document code:** A **Article ID:** 1005-1120(2025)06-0865-10

0 Introduction

With the widespread application of robots in industrial production and daily life, the multi-sensor data fusion is often involved in the robot control. In some complex environments, inertial measurement unit (IMU) modules are commonly used to compensate for core systems[1-4]. IMU is a core component that measures the motion state of an object through built-in inertial sensors. It can output the angular velocity and linear acceleration of the object in real time. Some advanced models can also directly output the attitude angles (such as Euler angles, quaternions), and are widely used in unmanned aircraft, autonomous driving, robots, aerospace, etc. It is a key technology for achieving "being able to sense one's own movement even without external reference". Li et al.[5] proposed a global navigation satellite system/inertial navigation system (GNSS/INS) tightly coupled positioning method to enhance the positioning accuracy of the carrier in harsh environments. Wei et al.[6] introduced a system error compensation to enhance the positioning accuracy and stability based on GNSS/IMU integrated navigation. In robot positioning and navigation problems, the calculation of robot attitude is often accompanied by it[7-8]. Therefore, the use of IMU-assisted repositioning method was proposed by Yang et al.[9] to enhance the accuracy of its positioning algorithm. Zhang et al.[10] utilized a tightly coupled approach to fuse multi-sensor data, which made the pose calculation for robots more accurate compared

*Corresponding author, E-mail address: 981554323@qq.com.

How to cite this article: LI Na, LI Kun, HE Haiyu, et al. Dynamic error suppression of inertial measurement unit based on improved unscented Kalman filter[J]. Transactions of Nanjing University of Aeronautics and Astronautics, 2025, 42(6): 865-874.

http://dx.doi.org/10.16356/j.1005-1120.2025.06.012

with single sensors. However, the accelerometers[11] and magnetometers in IMU chips of micro-electro-mechanical system (MEMS) are susceptible to the interference. Therefore, a more comprehensive filtering algorithm is needed to process the data.

Outputs from the raw data of the IMU system are the system angular velocity and linear acceleration, and based on these, a new algorithm is needed to calculate the attitude data of the system at the current moment. As calculation errors and measurement errors may occur in the hardware IMU chip, and if there is any vibration or any other forms of interference in the system, it is highly likely to cause significant angle errors, or even directly result in data anomalies, which can lead to more serious errors. During robot walking, due to the road bumps or vibrations generated by the body's power system, the outputs of accelerometers and magnetometers are interfered, which directly affects the filter output of the IMU[12-17]. Liu et al.[18] proposed that the accuracy of the output of attitude data from IMU can be improved with the adaptive unscented Kalman filtering (UKF) algorithm to adaptively adjust the initial values required by the filtering algorithm. But when the dimension of state variables in nonlinear systems is high, the UKF cannot better adapt to high-dimensional systems. Therefore, the fuzzy robust adaptive methods were put forward by Qiao et al.[19] to enhance the stability of the filter, and thus the cubature Kalman filter (CKF) algorithm is more suitable for high-dimensional systems compared with the UKF algorithm. Due to the fact that the susceptibility of inertial sensitive components such as accelerometers and gyroscopes are sensitive to vibration, Yang et al.[20] advanced the fusion of UKF algorithm and complementary filtering algorithm, which significantly improved the vibration resistance performance of IMU. The usage of UKF algorithm for the real-time estimation and calibration of magnetometers was proposed by Shen et al.[21] and Lu et al.[22], which improved the accuracy of heading angle estimation. In Ref.[21], the two-stage UKF algorithm was adopted to calibrate magnetometers in real time, significantly improving their anti-interference ability in magnetic environments.

Above studies all mentioned that the measurement errors of IMU sensors were difficult to determine or the outputs of accelerometers and magnetometers were affected by various types of vibrations. Based on these problems that IMU is sensitive to these interferences, and the measurement noise of sensors is difficult to model and theoretically eliminate, this paper proposes to adopt the Sage-Husa adaptive method to estimate the measurement noise of sensors in real time, so as to improve the attitude calculation accuracy of the UKF algorithm.

1 Sage-Husa Adaptive Strong Tracking Unscented Kalman Filter Algorithm

In order to improve the accuracy of the algorithm and adapt to measurement noise under different working conditions, an adaptive unscented Kalman algorithm based on the Sage-Husa adaptive method is proposed to work out the attitude angle of aircraft. The structural diagram of the attitude calculation system is shown in Fig.1, in which the state update data are provided by the gyroscope and combined with acceleration measurement and geomagnetic measurement. After calculating the measurement priori estimate, the innovation matrix and the Sage-Husa method are used to make suboptimal estimate of the measurement noise, and a re-estimation is introduced to ensure the positive definiteness of the measurement noise matrix. Finally, the Kalman gain is calculated and then the attitude angle is obtained.

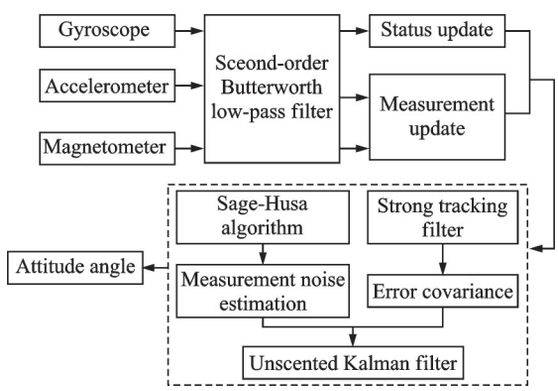

Fig.1 Structure diagram of the adaptive unscented Kalman filter system

1.1 State prediction and measurement equations for nonlinear systems

The nonlinear discrete state prediction equation for an IMU system is

$$\boldsymbol{X}_K = f(\boldsymbol{X}_{K-1}) + \boldsymbol{W}_{K-1} \tag{1}$$

where $\boldsymbol{X}_K$ and $\boldsymbol{X}_{K-1}$ respectively represent the priori estimate of the state variable at the time of K and the posterior estimate at the time of $K-1$; f denotes the nonlinear propagation of the system; and $\boldsymbol{W}_K$ is systematic error. $E[\boldsymbol{W}_K]=0$ is the variance matrix, and $E[\boldsymbol{W}_K, \boldsymbol{W}_K^{\mathrm{T}}]=\boldsymbol{Q}_K$ is the covariance matrix.

The measurement equation of the system is

$$\boldsymbol{Z}_K = h(\boldsymbol{X}_K) + \boldsymbol{V}_K \tag{2}$$

where $\boldsymbol{Z}_K$ represents the sensor measurements at the time of K, h the nonlinear propagation of the measurement equation, and $\boldsymbol{V}_K$ is measurement error. $E[\boldsymbol{V}_K]=\boldsymbol{V}_K$ is the variance matrix, and $E[\boldsymbol{V}_K, \boldsymbol{V}_K^{\mathrm{T}}]=\boldsymbol{R}_K$ represents the covariance matrix.

1.2 Unscented Transform and Kalman filtering framework

The unscented transform (UT) is a nonlinear transformation method based on the Cholesky decomposition, which can perform nonlinear propagation on the sampling points of the known data, thereby directly close to the statistical characteristics of the posterior date. Firstly, sample the state variables of the system, where the system state variables are represented as $\boldsymbol{X}_K = [q_0, q_1, q_2, q_3, \omega_X, \omega_Y, \omega_Z]^{\mathrm{T}}$. Among them, $\boldsymbol{q}$ is the quaternion vector and $\boldsymbol{\omega}$ the three-axis angular velocity vector. The sampling method for $\boldsymbol{X}_K$ is

$$\chi_{K-1} = \left[\hat{\boldsymbol{X}}_{K-1}\left[\hat{\boldsymbol{X}}_{K-1}\right]_n + \gamma\sqrt{\boldsymbol{P}_{X,K-1}}\left[\hat{\boldsymbol{X}}_{K-1}\right]_n - \gamma\sqrt{\boldsymbol{P}_{X,K-1}}\right] \tag{3}$$

where χ_{K-1} is the sampling matrix for system state variables, i.e. Sigma points; γ the scale parameter of the distribution of Sigma points; $\boldsymbol{P}_{X,K-1}$ the error priori covariance matrix, which is iterated after the initial values are given; $\hat{\boldsymbol{X}}_{K-1}$ the posterior value of the previous state variable, and n the dimension of the system state variables. The nonlinear propagation of the system χ_{K-1} is

$$\chi^*_{i,K|(K-1)} = f(\chi_{i,K-1}) \tag{4}$$

where $\chi^*_{i,K|(K-1)}$ represents the output of the system state variables after propagation. And the weight sum can be calculated as follows

$$\hat{\chi}_{K|(K-1)} = \sum_{i=0}^{2n} W_i^m \chi^*_{i,K|(K-1)} \tag{5}$$

where $\chi^*_{i,K|(K-1)}$ denotes the ith column of matrix $\chi^*_{K|(K-1)}$; W_i^m the weight value for each column of data, shown as

$$\begin{cases} W_0^m = \lambda/\gamma^2 \\ W_i^m = 1/2\gamma^2 \end{cases} \tag{6}$$

$$\lambda = \alpha^2(n+\kappa) - n \tag{7}$$

where α controls the distribution of Sigma points with the value of 1; and κ is used to ensure the semi-positive definiteness of $\boldsymbol{P}_{X,K-1}$, with the value of 0. At the present time, the current second priori estimate value of the state variables can be obtained as $\hat{\chi}_{K|(K-1)}$. The measurement vector for the system is $\boldsymbol{Y}_K = [q_0, q_1, q_2, q_3, \omega_X, \omega_Y, a_X, a_Y, a_Z, m_X, m_Y, m_Z]^{\mathrm{T}}$, with $\boldsymbol{a}$ as the three-axis acceleration vector, and $\boldsymbol{m}$ as the three-axis geomagnetic data. Performing the UT on them, the sampling matrix of the measurement vector is

$$\boldsymbol{\xi}_{K|(K-1)} = \left[\hat{\boldsymbol{X}}_{K|(K-1)}\left[\hat{\boldsymbol{X}}_{K|(K-1)}\right]_n + \gamma\sqrt{\boldsymbol{P}_{X,K|(K-1)}} \left[\hat{\boldsymbol{X}}_{K|(K-1)}\right]_n - \gamma\sqrt{\boldsymbol{P}_{X,K|(K-1)}}\right] \tag{8}$$

And the nonlinear propagation is measured on the sampling matrix.

$$\boldsymbol{\eta}_{i,K|(K-1)} = h(\chi_{i,K|(K-1)}) \tag{9}$$

where $\boldsymbol{\eta}_{i,K|(K-1)}$ is the output of the measured state variable after propagation, and its weight is calculated by

$$\hat{\boldsymbol{Y}}_{K|(K-1)} = \sum_{i=0}^{2n} W_i^m \boldsymbol{\eta}_{i,K|(K-1)} \tag{10}$$

where $\hat{\boldsymbol{Y}}_{K|(K-1)}$ is the measurement priori estimate value. Then the covariance matrix of system state variables, the measurement vector covariance matrix, and the covariance matrix of system state variables and measurement vector can be expressed as

$$\boldsymbol{P}_{X,K|(K-1)} = \sum_{i=0}^{2n} W_i^c\left(\chi^*_{i,K|(K-1)} - \hat{\boldsymbol{X}}_{K|(K-1)}\right)\times \left(\chi^*_{i,K|(K-1)} - \hat{\boldsymbol{X}}_{K|(K-1)}\right)^{\mathrm{T}} + \boldsymbol{Q}_{K-1} \tag{11}$$

$$\boldsymbol{P}_{Y,K|(K-1)} = \sum_{i=0}^{2n} W_i^c\left(\boldsymbol{\eta}_{i,K|(K-1)} - \hat{\boldsymbol{Y}}_{K|(K-1)}\right)\times \left(\boldsymbol{\eta}_{i,K|(K-1)} - \hat{\boldsymbol{Y}}_{K|(K-1)}\right)^{\mathrm{T}} + \boldsymbol{R}_K \tag{12}$$

$$\boldsymbol{P}_{XY,K|(K-1)}=\sum_{i=0}^{2n}W_i^c\left(\boldsymbol{\chi}_{i,K|(K-1)}-\hat{\boldsymbol{X}}_{K|(K-1)}\right)\times\left(\boldsymbol{\eta}_{i,K|(K-1)}-\hat{\boldsymbol{Y}}_{K|(K-1)}\right)^{\mathrm{T}} \tag{13}$$

where W_i^c is the measurement coefficients of error covariance matrix. $\boldsymbol{Q}_{K-1}$ and $\boldsymbol{R}_K$ are the covariance matrices for the system noise and measurement noise. Far from now, the UT is completed, and the values of $\boldsymbol{P}_{X,K|(K-1)}$, $\boldsymbol{P}_{Y,K|(K-1)}$, $\boldsymbol{P}_{XY,K|(K-1)}$, $\hat{\boldsymbol{Y}}_{K|(K-1)}$, and $\hat{\boldsymbol{\chi}}_{K|(K-1)}$ are substituted, which are calculated initially, into the Kalman filtering algorithm framework.

$$\boldsymbol{K}_K=\boldsymbol{P}_{XY,K|(K-1)}\boldsymbol{P}_{Y,K|(K-1)}^{-1} \tag{14}$$

$$\hat{\boldsymbol{X}}_K=\hat{\boldsymbol{X}}_{K|(K-1)}+\boldsymbol{K}_K\left(\boldsymbol{Z}_K-\hat{\boldsymbol{Y}}_{K|(K-1)}\right) \tag{15}$$

Finally, the priori error covariance matrix is updated and saved to complete the iteration.

$$\boldsymbol{P}_{X,K}=\boldsymbol{P}_{X,K|(K-1)}-\boldsymbol{K}_K\boldsymbol{P}_{Y,K|(K-1)}\boldsymbol{K}_K^{\mathrm{T}} \tag{16}$$

From Eqs.(11) and (12), it can be found that the covariance matrices $\boldsymbol{Q}_{K-1}$ and $\boldsymbol{R}_K$ are given as initial values based on engineering experience and are not iteratively calculated in engineering calculations. This will result in significant errors that cannot be accurately captured by the filter, leading to blind trust in the measured or predicted values. Due to the high degree of nonlinearity of the system equations, the system noise is difficult to estimate, and the output angular velocity of the gyroscope is relatively stable. Accordingly, the system noise is generally small. However, the accelerometers and magnetometers are highly susceptible to interference, so the estimation of measurement noise is chosen to compensate $\boldsymbol{P}_{Y,K|(K-1)}$ for the system. In real engineering environments, the sensitive characteristics of IMU sensors can easily generate outliers as measurement fault points. Therefore, a strong tracking filtering can be introduced to correct the error priori covariance matrix to improve the data utilization and filtering accuracy.

2 Improved UKF Algorithm Based on Adaptive Strong Tracking Filtering

Starting from the UKF algorithm model mentioned above, the innovation matrix $\boldsymbol{\varepsilon}_K$ can be worked out first by Eq.(10) and the current measured value $\boldsymbol{Z}_K$ of the sensor, and its variance matrix $\boldsymbol{\Gamma}_K$ can be expressed as

$$\boldsymbol{\Gamma}_K=\begin{cases}\boldsymbol{\varepsilon}_K\boldsymbol{\varepsilon}_K^{\mathrm{T}} & K=1\\ (1-\beta_K)\boldsymbol{\Gamma}_{K-1}+\beta_K\boldsymbol{\varepsilon}_K\boldsymbol{\varepsilon}_K^{\mathrm{T}} & K>1\end{cases} \tag{17}$$

$$\boldsymbol{\varepsilon}_K=\boldsymbol{Z}_K-\hat{\boldsymbol{Y}}_{K|(K-1)} \tag{18}$$

where $\beta_K=\dfrac{\beta_{K-1}}{\beta_{K-1}+b}$ $(0<b<1)$ is the exponential fading factor, $\beta_0=1$, and $\beta_\infty=1-b$. b is usually taken as 0.95—0.99. Then the measurement noise estimation formula can be obtained from the Sage-Husa adaptive method as follows

$$\hat{\boldsymbol{R}}_K=(1-\beta_K)\hat{\boldsymbol{R}}_{K-1}+\beta_K(\boldsymbol{\varepsilon}_K\boldsymbol{\varepsilon}_K^{\mathrm{T}}-\boldsymbol{P}_{Y,K|(K-1)}) \tag{19}$$

Due to the independence of measurement, $\hat{\boldsymbol{R}}_K$ is a positive definite diagonal matrix. Moreover, the latter term undergoes subtraction in Eq.(19), and during the iteration process, the value of $\boldsymbol{\varepsilon}_K\boldsymbol{\varepsilon}_K^{\mathrm{T}}$ becomes smaller and smaller as $\hat{\boldsymbol{R}}_K$ becomes more accurate, which may result in the iteration of $\hat{\boldsymbol{R}}_K$ being non-positive definite. Usually, this problem can be solved by adopting sequential filtering, but in robot control systems, the computing resources are limited and the real-time requirements are high. Therefore, it is necessary to make a judgment on the iterated $\hat{\boldsymbol{R}}_K$ here. If it is found to be non-positive definite, $\hat{\boldsymbol{R}}_K$ should be reassigned according to its initial value and re iterated. This not only solves the non-positive definite problems, but also enables $\hat{\boldsymbol{R}}_K$ to converge more flexibly in the different operating environments.

By introducing a fading factor λ_K, the strong tracking filtering corrects the priori covariance matrix of errors in the UKF algorithm, and the single fading factor λ_K can be expressed as

$$\lambda_K=\max\left[1,\frac{\mathrm{tr}(\boldsymbol{N}_K)}{\mathrm{tr}(\boldsymbol{M}_K)}\right] \tag{20}$$

where $\boldsymbol{N}_K=\boldsymbol{\Gamma}_K-\boldsymbol{R}_K$, $\boldsymbol{M}_K=\sum_{i=0}^{2n}W_i^c\left(\boldsymbol{\eta}_{i,K|(K-1)}-\hat{\boldsymbol{Y}}_{K|(K-1)}\right)\cdot\left(\boldsymbol{\eta}_{i,K|(K-1)}-\hat{\boldsymbol{Y}}_{K|(K-1)}\right)^{\mathrm{T}}$, and the corrected priori error covariance matrix can be expressed as

$$\boldsymbol{P}_{X,K}=\boldsymbol{\Lambda}_K\boldsymbol{P}_{X,K|(K-1)}\boldsymbol{\Lambda}_K-\boldsymbol{K}_K\boldsymbol{P}_{Y,K|(K-1)}\boldsymbol{K}_K^{\mathrm{T}} \tag{21}$$

where $\boldsymbol{\Lambda}_K=\boldsymbol{A}\,\mathrm{diag}(\sqrt{\lambda_k},\sqrt{\lambda_k},\sqrt{\lambda_k},\cdots)$, and $\boldsymbol{A}=\mathrm{diag}(\sqrt{a_1},\sqrt{a_2},\sqrt{a_3},\cdots)$ is the predetermined experience fading ratio coefficient. Here, a_1, a_2 and a_3 are the coefficients of the diagonal matrix and used to adjust the weights.

Due to the susceptibility of sensitive components such as accelerometers and gyroscopes to vi-

bration, they can output high-frequency clutter, which will cause estimation errors in filters and lead to misjudgments in decision-making systems. Therefore, a low-pass filter with a cutoff frequency of 50 Hz and a sampling frequency of 500 Hz is designed to help adaptive strong tracking unscented Kalman filter (ASTUKF) suppress the high-frequency signals with significant impact. To sum up, the algorithm steps can be summarized as follows.

Step 1 Apply infinite impulse response filter (IIRF) to the original observation signal to suppress high-frequency interference.

Step 2 Initialize the state vector, the error covariance matrix, the process noise covariance matrix and the measurement noise covariance matrix. Furthermore, initialize the adaptive parameters and the strong tracking factor.

Step 3 Based on the state vector and the error covariance matrix, generate the Sigma point set using a symmetric strategy.

Step 4 Perform nonlinear propagation on the Sigma point set and predict the state vector based on the nonlinear system.

Step 5 Predict the measurement vector and calculate the innovation matrix.

Step 6 Calculate the strong tracking fading factor and update the error covariance matrix.

Step 7 Calculate the Kalman gain, estimate the system state vector and update the error covariance matrix.

The algorithm proposed in this paper has a higher overall complexity than the traditional extended Kalman filter (EKF) and basic UKF, but it still falls within the range of real-time feasibility for engineering applications. The IIRF introduces linear complexity, while the complexity of ASTUKF mainly stems from UT, strong tracking factor calculation, and Sage-Husa adaptive noise estimation. Overall, it is of the order of $O(n^2)$ regarding the system state dimension n, which is suitable for the real-time requirements of low-cost MEMS IMUs.

3 Experimental Verification and Data Analysis

3.1 Experimental platform

In order to verify the correctness of the proposed method, a hardware testing platform was constructed using the STM32H743 microcontroller, the six-axis gyro accelerometer ICM20689, and the three-axis magnetometer QMC5883L. The hardware parameters are shown in Table 1.

Table 1 Parameters of six-axis gyro accelerometer ICM20689 and three-axis magnetometer QMC5883L

Sensor type	Resolution	The maximum measurement range
Accelerometer	4 096 LSB/g	$\pm 8g$
Gyroscope	16.4 LSB/((°)•s^{-1})	2 000 (°)/s
Magnetometer	3 000 LSB/Gs	±8 Gs

Note: LSB means the least significant bit.

The output data of ICM20689 include 16-bit three-axis accelerometer and six-axis gyroscope data, which are read by the main controller through the SPI communication protocol. The 16-bit three-axis geomagnetic data, provided by the QMC5883L chip, are read by the main controller through the inter-integrated circuit (IIC) communication protocol. After reading the raw data, the data calculation is performed in the main controller, and finally the data are uploaded to the PC to be processed by MATLAB.

3.2 Comparison experiments

3.2.1 Data comparison during IMU in static state

An experience was conducted by using the STM32H743 microcontroller to implement EKF, UKF, ASTUKF, and infinite impulse response-ASTUKF (IIR-ASTUKF), and the comparison are made among those data. The sampling frequency of the system is 500 Hz, and the samples are from the roll, pitch, and yaw axes. 30 000 sampling points are sampled on each axis, and the root mean square error (RMSE) of each filtering algorithm is calculated by the true values of the data to evaluate the accuracy of the output angle. Figs.2(a, c, e) show the angle output curves of the roll axis, pitch axis, and yaw axis, respectively. And the corresponding angle errors of the roll axis, pitch axis, and yaw axis are respectively displayed in Figs.2(b, d, f). The Fourier transform is performed on the filtered angle data, and then their spectrums are obtained, which can be seen in Fig.3. The comparison of RMSEs of the three axis angles is shown in Table 2.

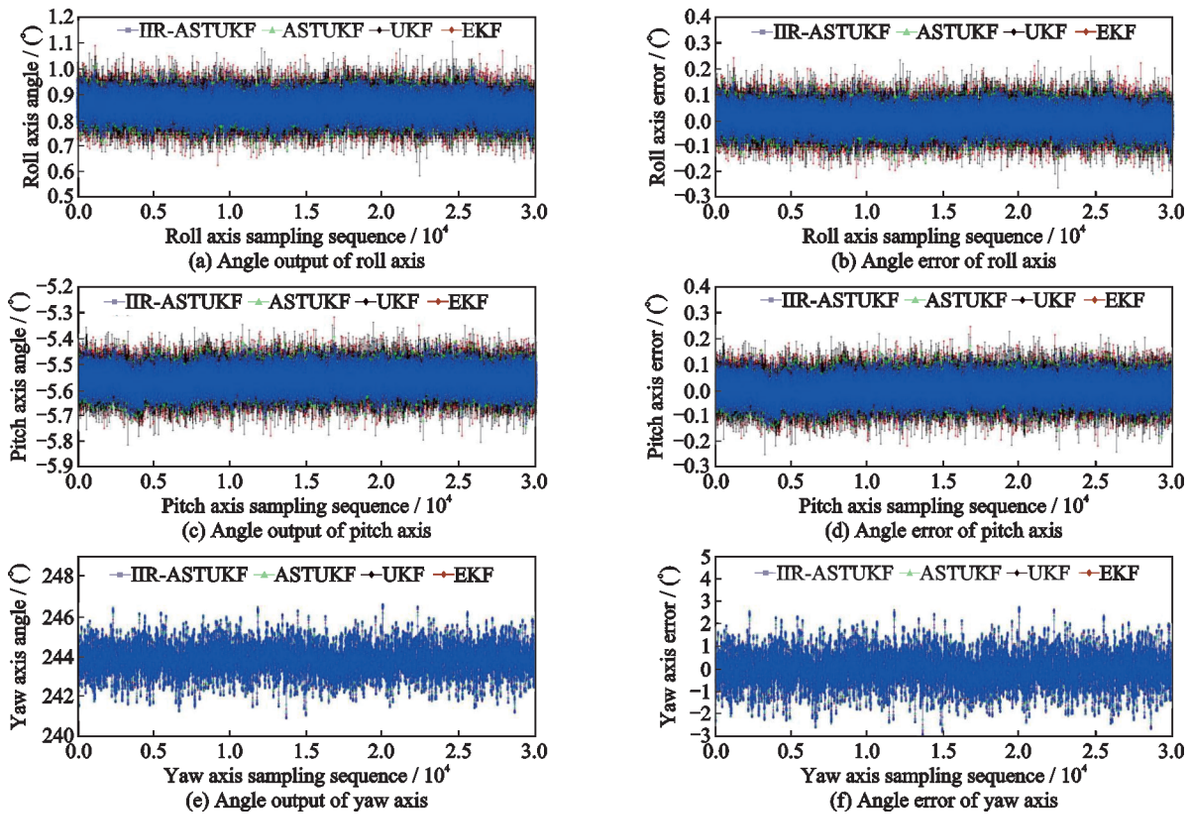

Fig.2 Three-axis attitude changes and measurement errors when IMU is in static state

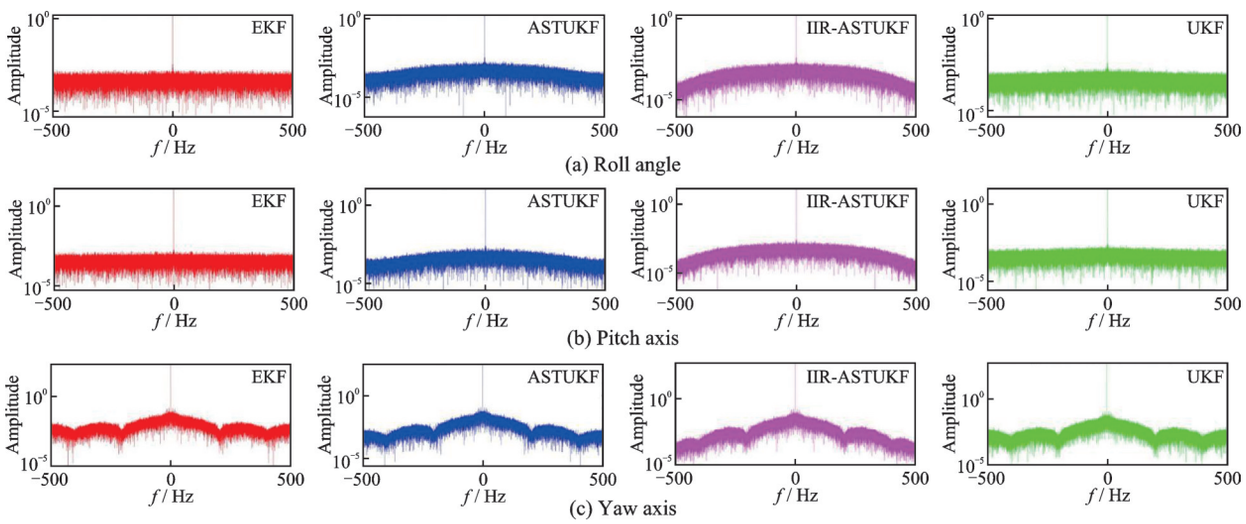

Fig.3 Three-axis spectrum of IMU in static state

Table 2 RMSE comparison when IMU is in static state

(°)

Attitude angle	EKF	UKF	ASTUKF	IIR-ASTUKF
Roll axis	0.003 4	0.002 8	0.001 7	0.001 6
Pitch axis	0.003 5	0.002 8	0.001 8	0.001 7
Yaw axis	0.573 8	0.554 7	0.536 5	0.534 6

Fig.3 shows that when the sensor is in a static interference environment, its output assignment of the normal data is not affected, but as the frequency increases, the amplitude of the data output gradually decreases. It should be noticed that the frequency of the data output in this experiment is beyond 50 Hz. When in higher frequencies from 50 Hz to 500 Hz, the interference signals can be greatly suppressed. Therefore, in the static state, the higher the frequency is, the relatively smaller the jumps of the output data are, and the more remarkable its ability to suppress interference is. This further verifies the validity and effectiveness of the algorithm

proposed in this paper.

When IMU is in a static state, the data variance can also be used to evaluate the degree of dispersion of the data relative to the true value. Therefore, as shown in Fig.2, the variances of the rolling axis in EKF, UKF, and our algorithms are 0.058 31, 0.052 64, and 0.040 62, respectively; the variances of the pitch axis in EKF, UKF, and our algorithms are 0.058 93, 0.052 49, and 0.040 65, respectively; and the variances of the yaw axis in EKF, UKF, and our algorithms are 0.757 5, 0.744 8, and 0.731 2, correspondingly. Compared with the traditional algoithms of EKF and UKF, the algorithm advanced in this paper tends to be much closer to the true value in static state. Moreover, it can be found from Table 2 that RMSEs of the three-axis data calculated by the algorithm in this paper are relatively small. Therefore, compared with the traditional algorithms of EKF and UKF, our algorithm has higher estimation accuracy in static state.

3.2.2 Comparison of measurement data during IMU in motion

In order to be close to the actual working conditions, the unmanned vehicle is used as the experimental platform to detect the anti-vibration interference ability of the IMU system. The experimental platform of the unmanned vehicle is shown in Fig.4.

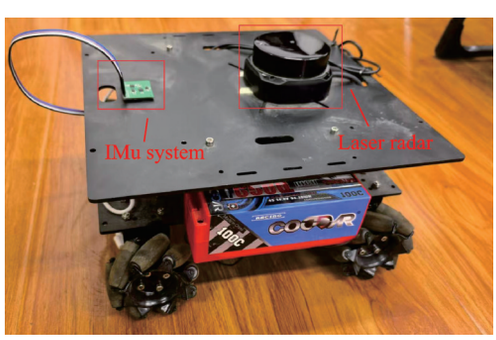

Fig.4 Unmanned vehicle experimental platform

When the IMU system is working normally, an order is given to make the roll and pitch angles in IMU move freely within $\pm 50^{\circ}$, and the yaw angle move freely between 240° and 360° at the frequency of 500 Hz. Then the roll, pitch, and yaw axes are sampled separately, and each 10 000 sampling points are sampled for the purpose that the accuracy of the output angle can be evaluated by calculating RMSEs of each filtering algorithm with the true values of the data. Figs.5(a, c, e) show the angle output curves of the roll axis, pitch axis, and yaw axis, respectively. And the angle errors of the roll axis, pitch axis, and yaw axis are presented in Figs.5(b, d, f) correspondingly. Then the Fourier transform is performed on the filtered angle data to obtain their spectrums, shown in Fig.6. Moreover, the comparison of RMSEs of the three axis angles is shown in Table 3.

From Figs.5(a, c, e), it can be seen that in contrast to traditional EKF and UKF algorithms, the attitude angle curve worked out by the algorithm put forward in this paper is much smoother. In the process of IMU motion, due to the real-time adaptive measurement noise and the correction effect of strong tracking algorithms on priori error covariance, more accurate reference is provided for the Kalman gain calculation in UKF. On the other hand, as shown in Figs.5(b, d, f), our algorithm has the smallest error among the three algorithms.

Fig.6 shows that when the sensor is in a dynamic interference environment, its data output assignment is not actually affected, but as the frequency increases, the data output amplitude gradually decreases. During the dynamic conditions, the output data of the sensor may experience significant fluctuations. However, compared with the static conditions, the normal output of data is prioritized for assurance, resulting in less suppression of high-frequency signals. But compared with traditional algorithms, its anti-interference ability is superior near the frequency of 500 Hz.

Moreover, from Table 3, it can be concluded that RMSEs of the three axes in the algorithm proposed in this paper are relatively small. Therefore, under normal measured motion conditions, the algorithm proposed in this paper has more advantages and higher estimation accuracy. Due to the small and high frequency vibration in the movement of the vehicle IMU system, the unmanned vehicle platform shown in the test system has a rigid connection between the IMU and the vehicle body, and no buffer processing is done. This leads to that the interference of the vehicle body vibration will be directly transmitted to the IMU system, resulting in more serious interference or error. However, it can be

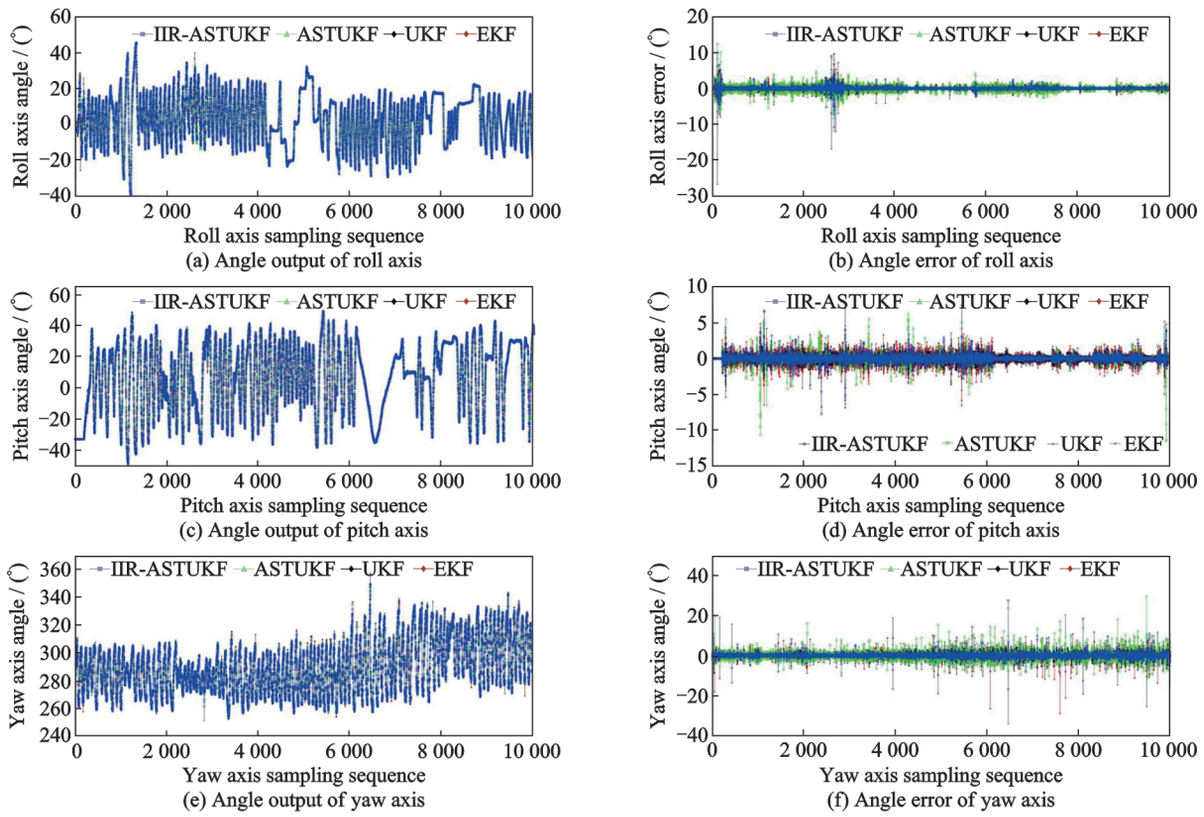

Fig.5 Three-axis attitude changes and measurement errors during IMU in motion

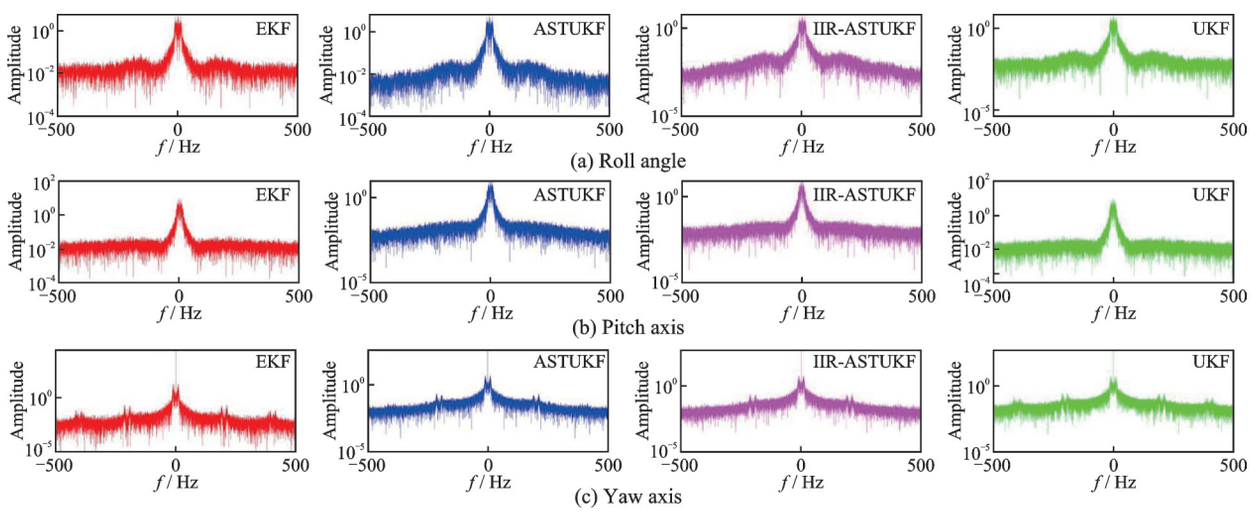

Fig.6 Three-axis spectrum during IMU in motion

Table 3 RMSE camparison when IMU is in motion

(°)

Attitude angle	EKF	UKF	ASTUKF	IIR-ASTUKF
Roll axis	0.630 4	0.419 6	0.278 5	0.178 0
Pitch axis	0.459 6	0.394 1	0.318 7	0.191 0
Yaw axis	3.152 2	2.232 9	1.690 6	0.830 6

seen from Fig.5 that the angle output data are normal and there are few outliers in the measured data values, which can be used to guide the navigation of unmanned vehicles. It can also illustrate the suppression effect of the proposed algorithm for high-frequency interference signals.

4 Conclusions

When solving IMU data, the EKF algorithm can solve the nonlinear problems of the system, but it also introduces errors in high-order Taylor terms and operations of Jacobian matrix, resulting in a large computational workload for EKF. By the

method of approximating the posterior probability statistical characteristics of variables, the UKF algorithm improves the above problems, however, it can cause significant errors when the measurement noise cannot be accurately obtained. This paper proposes a second-order Butterworth low-pass filter to process sensor raw data, avoiding interference from outliers and high-frequency noise. On this basis, the Sage-Husa adaptive method is introduced to improve the UKF algorithm so as to estimate measurement noise while iterating the algorithm. The Sage-Husa adaptive method is only a suboptimal estimation, but it can estimate noise based on the read measurement data and update the measurement noise with historical information. Pleasantly, it can solve the problem of outliers in actual systems through strong tracking filtering. This method significantly improves the filtering accuracy of the system without reducing data utilization. Moreover, the RMSE in the proposed algorithm is the smallest compared to EKF and UKF, which can meet the measurement requirements of low-cost MEMS IMU systems and is applicable to unmanned vehicles or unmanned aerial vehicle systems.

References

[1] GROVER S, SAHU C, PODDAR S. Linear likelihood approach-based adaptive fusion of heterogeneous multiple IMUs for orientation estimation[J]. IEEE Sensors Journal, 2024, 24(15): 24512-24519.

[2] ZAKARIA W N W, SHAMSUDIN A U, RAHMAN M A A, et al. ROS-based SLAM and path planning for autonomous unmanned surface vehicle navigation system[C]//Proceedings of 2022 IEEE 5th International Symposium in Robotics and Manufacturing Automation (ROMA). Malacca, Malaysia: IEEE, 2022: 1-6.

[3] AI Z, WANG Z, CUI W. Low-power wireless wearable ECG monitoring chestbelt based on ferroelectric microprocessor[C]//Proceedings of 2019 Chinese Control Conference (CCC). Guangzhou, China: [s.n.], 2019: 6434-6439.

[4] NIQUILLE S C. Regarding the pain of SpotMini: Or what a robot's struggle to learn reveals about the built environment[J]. Architectural Design, 2019, 89(1): 84-91.

[5] LI Bofeng, CHEN Guange. Collaborative precision positioning method of vehicle based on GNSS/INS [J]. Acta Geodaetica et Cartographica Sinica, 2022, 51(8): 1708-1716. (in Chinese)

[6] WEI Wenhui, ZHAO Xiangmo, GE Zhenzhen. GNSS/IMU combined positioning algorithm for intelligent vehicle considering dynamic model system error compensation[J]. China Journal of Highway and Transport, 202,35(9): 185-194. (in Chinese)

[7] JIANG F Y, CHENG Y, WANG H Z, et al. An engineering solution for multi-sensor fusion SLAM in indoor and outdoor scenes[C]//Proceedings of 2024 43rd Chinese Control Conference (CCC). Kunming, China: [s.n.], 2024: 4522-4528.

[8] PATEL U N, FARUQUE I A. Sensor fusion to improve state estimate accuracy using multiple inertial measurement units[C]//Proceedings of 2021 IEEE International Symposium on Inertial Sensors and Systems (INERTIAL), Kailua-Kona, HI, USA: IEEE, 2021: 1-4.

[9] YANG Weili, LUO Dachan, CHEN Chaomeng, et al. Research on fast camera relocation method based on IMU[J]. Computer Simulation, 2022, 39(5): 413-417. (in Chinese)

[10] ZHANG Fubin, WANG Kai, LIAO Weifei, et al. Lidar/MEMS IMU/odometer compact integrated navigation algorithm[J]. Chinese Journal of Scientific Instrument, 202,43(7): 139-148. (in Chinese)

[11] ZHANG X, WU Q, SUN H. A data fusion method based on an optimized neural network for MEMS accelerometer arrays[C]//Proceedings of 2024 5th International Conference on Big Data & Artificial Intelligence & Software Engineering (ICBASE).Wenzhou, China: [s.n.], 2024: 34-37.

[12] BAN L, YANG C, LIU J, et al. Algorithm design of perception and navigation for unmanned vehicles based on multi-sensor fusion and co-location[C]//Proceedings of 2023 International Conference on Ambient Intelligence, Knowledge Informatics and Industrial Electronics (AIKIIE). Ballari, India: [s.n.], 2023: 1-5.

[13] MAGAD A, EMZIR M. A magnetic field SLAM algorithm based on Bayesian filtering and gaussian process regression[C]//Proceedings of 2024 18th International Conference on Control, Automation, Robotics and Vision (ICARCV). Dubai, United Arab Emirates: [s.n.], 2024: 739-743.

[14] FEMINE A D, GALLO D, IODICE C, et al. Improving kinematic measurements in indoor sport applications through EKF-based UWB/IMU fusion[C]// Proceedings of 2024 IEEE International Workshop on Metrology for Industry 4.0 & IoT (MetroInd4.0 & IoT). Firenze, Italy: [s.n.], 2024: 333-338.

[15] SZCZEPANIAK J, SZLACHETKO B. Close-distance optical flow fusion using EKF for multirotor UAV position estimation[C]//Proceedings of 2023 Signal Processing Symposium (SPSympo). Karpacz, Poland: [s.n.], 2023: 180-183.

[16] CAI Anjiang, LIU Kaifeng, LIU Libo, et al. Adaptive DUKF attitude estimation algorithm for multi-rotor UAV[J]. Machinery Design & Manufacture, 2021(6): 284-287. (in Chinese)
[17] LI Na, HE Haiyu, JING Min, et al. IMU dynamic error suppression based on improved EKF[J]. Journal of Nanjing University of Aeronautics & Astronautics, 2023, 55(4): 718-724. (in Chinese)
[18] LIU Kangan, ZHANG Weiwei, XIAO Yongchao, et al. Attitude calculation of four-rotor UAV based on adaptive untraceless Kalman filter[J]. Electro-optics and Control, 2022, 29(7): 126-131. (in Chinese)
[19] QIAO Meiying, GAO Yifei, LI Wanni, et al. MEMS-IMU attitude estimation based on fuzzy robust adaptive CKF algorithm[J]. Chinese Journal of Inertia Technology, 2022, 30(3): 296-303. (in Chinese)
[20] YANG Hai, FENG Xuanzhang, SHAN Daiwei, et al. Borehole deviation dynamic measurement method of IMU while drilling based on UKF and complementary filter[J]. Chinese Journal of Inertia Technology, 2022, 30(2): 141-147. (in Chinese)
[21] SHEN Yue, SUN Zhiwei, SHEN Yayun, et al. UKF two-level attitude estimation algorithm for linear plant protection UAV[J]. Transactions of the Chinese Society for Agricultural Machinery, 2022, 53(9): 151-159. (in Chinese)
[22] LU Yongle, WANG Wenxin, FENG Tao, et al. Pedestrian navigation algorithm based on online calibration of magnetometer[J]. Electronic Measurement Technique, 2022, 45(5): 44-48. (in Chinese)

Acknowledgements This work was supported by the Key Research and Development Program of Shaanxi Province (No.2024NC-YBXM-246), the Shaanxi Provincial Science and Technology Department (No.2024JC-YBQN-0725), the Education Department of Shaanxi Province (No. 23JK0371), and the Shaanxi University of Technology (No. SLGRCQD2318).

Authors

The first author Ms. **LI Na** received the B.S. degree in computer science and application from Shaanxi University of Technology in 2002 and the M.S. degree in computer application technology from Xidian University in 2008. Since 2002, she has been working at School of Mathematics and Computer Science of Shaanxi University of Technology. She is currently an associate professor. Her research mainly focuses on intelligent optimization algorithms, network information processing and related fields.

The corresponding author Mr. **HE Haiyu** received the M.S. degree in electric engineering from Shaanxi University of Technology in 2025. Since 2025, he has been working at Shaanxi University of Technology. He is currently a teaching assistant. His research interests include Kalman filtering and isolated switching power supplies.

Author contributions Ms. **LI Na** designed the study, improved the ASTUKF algorithm based on adaptive strong tracking filter, conducted the analysis, interpreted the results, and wrote the manuscript. Mr. **LI Kun** designed the structure of the adaptive untraced Kalman filter system. Mr. **HE Haiyu** contributed to data for the analysis of IMU measurement data. Prof. **JING Min** contributed to the discussion and background of the study. All authors commented on the manuscript draft and approved the submission.

Competing interests The authors declare no competing interests.

(Production Editor: ZHANG Huangqun)

基于改进无损卡尔曼滤波的惯性测量单元动态误差抑制

李 娜[1], 李 坤[1], 贺海育[2], 景 敏[3]

(1.陕西理工大学数学与计算机科学学院,汉中 723000,中国; 2.陕西理工大学特莱恩工学院,汉中 723000,中国; 3.陕西理工大学机械工程学院,汉中 723000,中国)

摘要:为提高机器人的位姿估计精度以及数据解算的稳定性,提出了一种量测噪音自适应强跟踪无损卡尔曼滤波(Adaptive strong tracking unscented Kalman filter,ASTUKF)算法。为了抑制高频噪音,该算法在ASTUKF前端引入一种无限冲激响应滤波器(Infinite impulse response filter,IIRF)对原始数据做预处理;然后在滤波的过程中对误差协方差矩阵进行修正,并对量测噪音进行估计;最后在搭建的硬件实验平台上进行测试。实验结果表明:本文算法数据解算横滚轴结果的均方根误差(Root mean square error, RMSE)较传统扩展卡尔曼滤波(Extended Kalman filter,EKF)和无损卡尔曼滤波(Unscented Kalman filter, UKF)算法分别降低了约57.5%、36.1%;俯仰轴结果的RMSE较传统EKF和UKF算法分别降低了约58.4%、51.5%;偏航轴结果的RMSE较传统EKF和UKF算法分别降低了约62.8%、50.9%。结果表明本文算法增强了抗高频振动干扰的能力,提高了姿态解算精度。

关键词:加速度计;惯性测量单元;自适应强跟踪无损卡尔曼滤波;四元数;卡尔曼滤波器